Int. J. Electrochem. Sci., 16 **(2021)** Article Number: 211133, doi: 10.20964/2021.11.30

International Journal of
ELECTROCHEMICAL
SCIENCE
www.electrochemsci.org

Preparation of Co-electrodeposited Pd-Au Nanocatalyst for Methanol Electro-oxidation

Yaser M. Asal [1], *Ahmad M. Mohammad* [2], *Sayed S. Abd El Rehim* [3], *Islam M. Al-Akraa* [1,*]

[1] Department of Chemical Engineering, Faculty of Engineering, The British University in Egypt, Cairo 11837, Egypt
[2] Chemistry Department, Faculty of Science, Cairo University, Cairo 12613, Egypt
[3] Chemistry Department, Faculty of Science, Ain Shams University, 11566 Abbassia, Cairo, Egypt
[*]E-mail: islam.ahmed@bue.edu.eg; islam0886@yahoo.com

Received: 2 August 2021 / *Accepted:* 9 September 2021 / *Published:* 10 October 2021

This investigation displayed the excellent electro-catalytic performance of methanol electro-oxidation reaction (MOR) in an alkaline medium at a binary catalyst composed of Pd (PdNPs) and Au (AuNPs) nanoparticles that were simultaneously electrodeposited onto a glassy carbon (GC) surface. The effect of the molar ratios of both Pd^{2+} and Au^{3+} salts in the deposition bath on the catalytic activity and stability of MOR at the as-prepared catalyst was evaluated. The Pd_1Au_1 catalyst (that was developed with Pd^{2+} and Au^{3+} salts of a 1:1 molar ratio) acquired the highest activity toward MOR in terms of the highest peak current density (I_p, 1.53 mA cm^{-2} compared to 0.13 mA cm^{-2} of the "pristine" Pd/GC (abbreviated as Pd_1Au_0) catalyst) with a significant (ca. – 50 mV) shift in onset potential of MOR. Furthermore, the Pd_1Au_1 catalyst classified the most durable; sustaining a stable current density of 0.20 mA cm^{-2} in 0.1 M NaOH solution containing 0.3 M methanol at 0 V after continuous electrolysis for 45 min (the corresponding current density of the Pd_1Au_0 catalyst was 0.04 mA cm^{-2}).

Keywords: Fuel cells; Methanol oxidation; Electrocatalysis; Pd-Au Co-deposition; Poisoning

1. INTRODUCTION

Due to the huge global growth in population, fossil fuels depletion and several environmental complications related to fossil fuels combustion, research has recently been devoted to explore other efficient energy resources capable to fulfil the increasing energy demands [1-8]. Of these resources, the direct liquid fuel cells (DLFCs) appeared promising in the direct conversion of the chemical energy into electricity with minor harmful emissions [9-15]. The direct methanol fuel cells (DMFCs) represented the simplest and safest realization of DLFCs with only a single carbon atom in the fuel's molecular structure. These DMFCs retained as well a low cost, low operating temperature, high energy and power densities, large fuel's availability and convenient and safe fuel's transportation and handling [16-21]. Its

theoretical volumetric energy density is ca. 4690 Wh L^{-1}) which is almost twice that of the direct formic acid fuel cells (2086 Wh L^{-1}) [22, 23]. Nevertheless, the sluggish oxidation kinetics of MOR and the proper selection of a propitious and durable catalyst of a low price for MOR remained challenging the movement of the DMFCs into a real commercialization.

Normally, Pt represented the most common electrocatalyst for several electrochemical oxidation processes particularly for oxygen evolution [24, 25] and for the oxidation of small organic fuels (methanol, formic acid, ethylene glycol, ..etc.) [11, 22, 26-29] and the literature is rich for these subjects. However, because of its high cost and susceptibility for potential poisoning by reaction intermediates (as CO), Pd (of a lower cost and a higher tolerance against CO poisoning) was instead proposed for fuel cells applications [30-32]. Yet, overcoming the CO poisoning effectively necessitated blending Pd with other transition metals such as Au [33], Ru [34], Fe [35], Co [36] and Ni [37] and sometimes with transition metal oxides as NiOx and MnOx [38-40]. This blending/modification endured the responsibility of preparing the Pd surface structurally, geometrically, and/or electronically to prohibit the CO adsorption or to boost its oxidative desorption at relatively low overpotentials.

In a continuation of this effort, we report, herein, on the development of a simultaneously co-electrodeposited Pd-Au nanocatalyst that was assembled onto a GC surface for MOR. The virtue of using the Co-electrodeposition technique to prepare the catalyst was discussed and several electrochemical and materials characterization techniques assisted in the evaluation of the morphology, composition and structure and further the activity and stability of the catalyst. A special emphasis was dedicated while preparing the catalyst to analyze the role of mixing the Pd^{2+} and Au^{3+} salts in different molar ratios in the deposition bath on the catalytic performance toward MOR.

2. EXPERIMENTAL

2.1. Electrodes and reagents

In this study, the working electrodes/catalysts were all assembled onto a cleaned GC (d = 5.0 mm) substrate and served in the electrochemical setup as working electrodes. A conventional cleaning treatment was applied for the GC substrate before using [41, 42]. In the same setup, an Ag/AgCl/NaCl (3M) and a spiral Pt wire were used as a reference and counter electrodes, respectively. Highly purified palladium (II) acetate (trimer, Pd 45.9 - 48.4%), hydrogen tetrachloroaurate (III) trihydrate (99.99% metals basis, Au 49.0%), sulphuric acid (98.0 %) and methanol (anhydrous, 99.0%) were purchased from Alfa Aesar and Sigma Aldrich.

2.2. Catalyst's fabrication

The simultaneous co-electrodeposition technique was employed for the fabrication of the catalysts [28, 29]. The deposition electrolyte was composed of 0.1 M Na_2SO_4 aqueous solutions that contained 2.0 mM $Pd(CH_3COO)_2$ and 2.0 mM $HAuCl_4$. For all catalysts, the electrodeposition of PdNPs and AuNPs onto the GC electrode surface was carried out potentiostatically at −0.2 V permitting the

passage of only 10 mC. The catalysts abbreviated as Pd_1Au_0, $Pd_1Au_{0.2}$, $Pd_1Au_{0.4}$, $Pd_1Au_{0.6}$, $Pd_1Au_{0.8}$ and Pd_1Au_1 reflected the deposition of PdNPs and AuNPs from deposition baths containing Pd^{2+} and Au^{3+} with molar ratios of 1:0, 1:0.2, 1:0.4, 1:0.6, 1:0.8 and 1:1, respectively.

2.3. Materials characterization and electrochemical measurement

The morphological and compositional information of the proposed catalysts was explored using the field emission scanning electron microscope (FE-SEM, FEI, QUANTA FEG250, Thermo Fisher) and energy dispersive X-ray spectroscopy (EDS, accelerating voltage of ca. 30 kV, original magnification was ×500, ISIS Company, England), respectively.

All electrochemical experiments were measured at a room temperature in a traditional three-electrode glass cell using a Bio-Logic SAS Potentiostat (model SP-150) that was operated with EC-Lab software. The real surface area of the catalysts was calculated from their corresponding cyclic voltammograms (CVs) in 0.5 M H_2SO_4 using a reference charge of ca. 420 μC cm^{-2} [43, 44].

3. RESULTS AND DISCUSSION

3.1. Surface morphology and composition

The surface morphological information (Fig. 1) was obtained for two catalysts; Pd_1Au_0 (bare, unmodified, Fig. 1A) and Pd_1Au_1 (of 1:1 Pd^{2+}:Au^{3+} ions, of the best catalytic performance toward MOR, vide infra, Fig. 1B) using the FE-SEM. Figure 1A confirmed the successful electrodeposition of spherical PdNPs with an average particle size of ca. 140 nm.

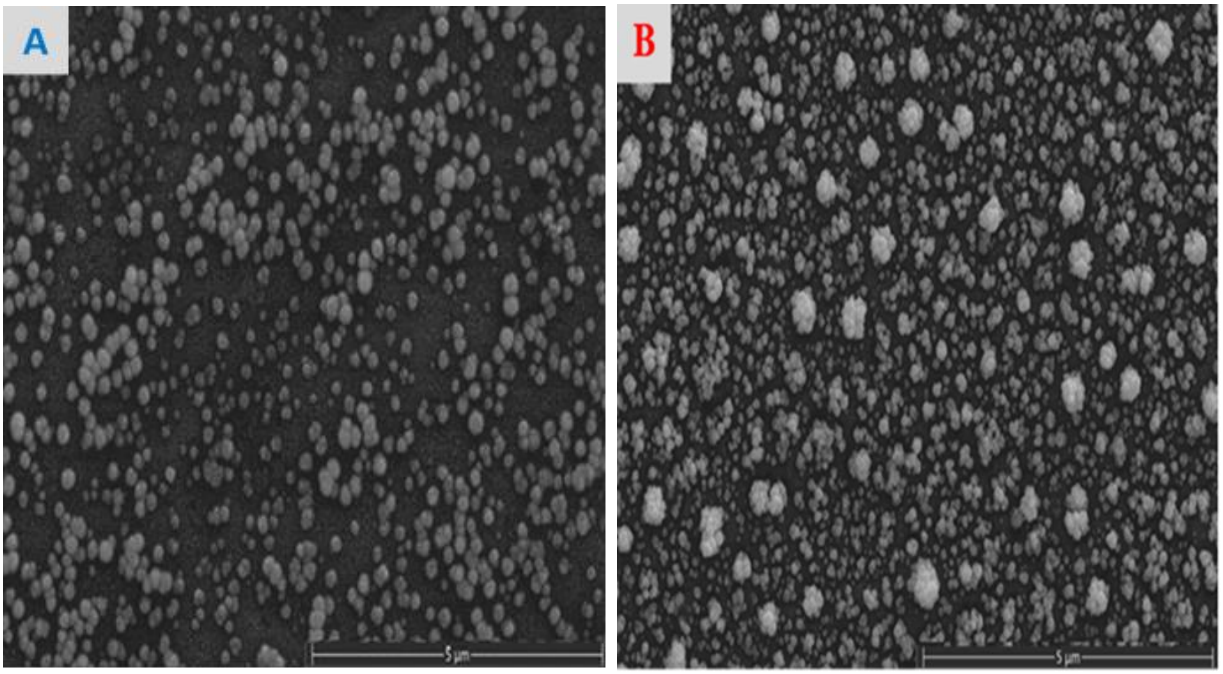

Figure 1. FE-SEM images of (A) Pd_1Au_0 and (B) Pd_1Au_1 catalysts.

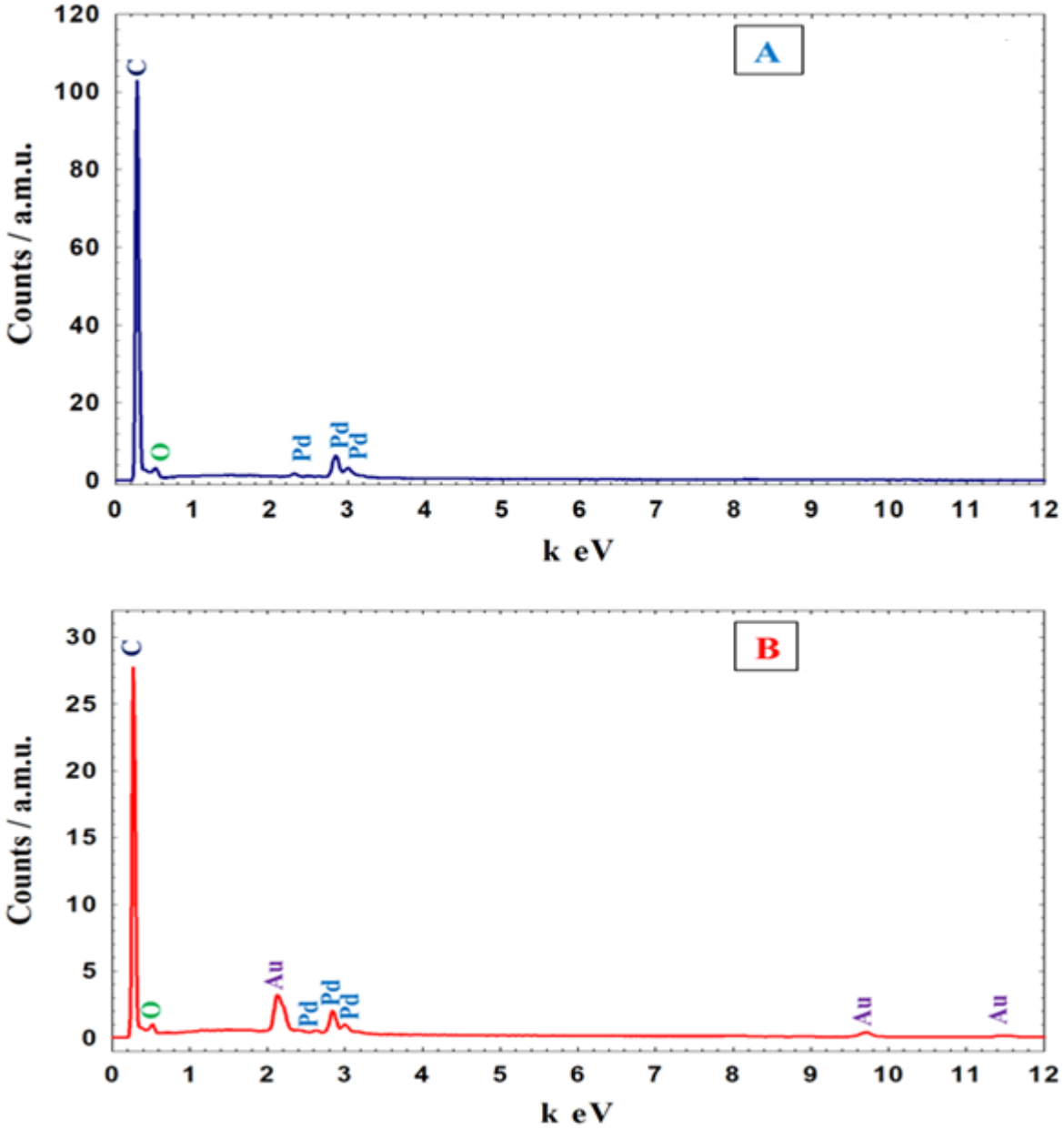

Figure 2. EDS spectra of (A) Pd_1Au_0 and (B) Pd_1Au_1 catalysts.

These nanoparticles appeared clustered and a bit enlarged (ca. 190 nm in average particle size) in the Pd_1Au_1 catalyst (Fig. 1B). These particles were aggregated a little in some areas. No distinction could be observed for the Pd and Au particles which inferred the possible alloying. The increase in the particle size of the Pd_1Au_1 catalyst suggested a role for Au^{3+} ions to speed up the particles' growth rates on the expense of their nucleation rates.

The EDS analysis of the Pd_1Au_0 catalyst (Fig. 2A) confirmed the electrodeposition of PdNPs onto the GC surface and the characteristic peaks of C, O and Pd appeared in their normal positions. On the other hand, the Pd_1Au_1 catalyst (Fig. 2B) preserved the previous peaks with another one for Au which ensured the inclusion of both PdNPs and AuNPs in the Pd_1Au_1 catalyst.

3.2. Electrochemical characterization

Electrochemical characterization is another important sensitive tool for the surface characterization of the catalyst. It sometimes provides fine details about the catalyst's ingredients that many materials characterization techniques miss them. Figure 3 shows the CVs measured in 0.5 M H_2SO_4 for the (a) Pd_1Au_0, (b) $Pd_1Au_{0.2}$, (c) $Pd_1Au_{0.4}$, (d) $Pd_1Au_{0.6}$, (e) $Pd_1Au_{0.8}$, and (f) Pd_1Au_1 catalysts in a potential range between − 0.2 to 1.5 V. Figure 3a (Pd_1Au_0 catalyst) depicted the typical characteristic response of a cleaned and pure Pd surface in acidic media in which the Pd oxidation peak extended from ca. 0.5 to 1.4 V and coupled with the Pd oxide (PdO) reduction peak at ca. 0.23 V [27, 45]. Additionally, the adsorption/desorption peaks of H_2 ($H_{ads/des}$) appeared in the potential range between ca. – 0.2 and 0.0 V. On the other side, three more observations were noticed after the simultaneous co-electrodeposition of AuNPs with PdNPs (in Fig. 3b-f):

- new anodic and cathodic peaks at ca. 0.8 V corresponding, respectively, to the Au oxidation (Au→AuO) and its subsequent (AuO→Au) reduction [29, 46] .
- decreasing the (PdO→Pd) and increasing the (AuO→Au) peak current intensities with increasing the amount of Au^{+3} ions in the deposition bath. This of course corresponded to lowering the real surface area of the active Pd surface (see Table 1).
- a positive shift in the peak potential of the (PdO→Pd) reduction that increased with the amount of Au^{+3} ions in the deposition bath. This confirm the alloying of the PdNPs and AuNPs with an observable change in the electronic properties of the Pd surface [47].
-

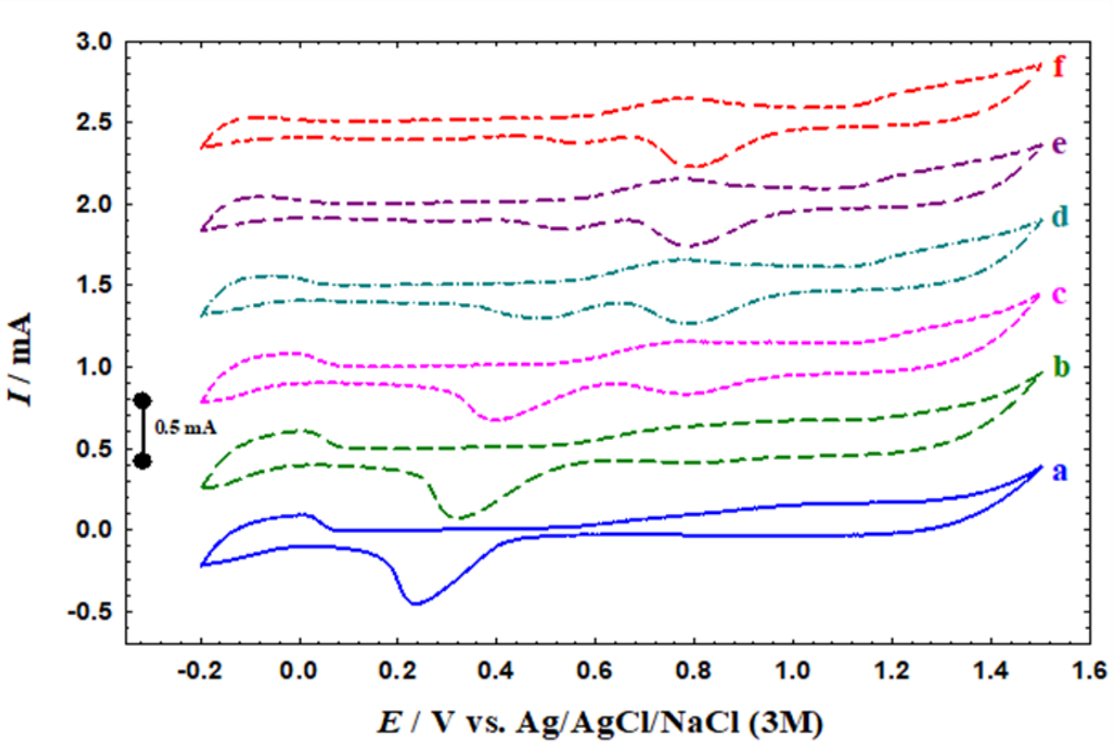

Figure 3. CVs measured in 0.5 M H_2SO_4 at (a) Pd_1Au_0, (b) $Pd_1Au_{0.2}$, (c) $Pd_1Au_{0.4}$, (d) $Pd_1Au_{0.6}$, (e) $Pd_1Au_{0.8}$, and (f) Pd_1Au_1 catalysts. (Potential scan rate = 100 mV s^{-1}).

Table 1. Estimated real surface area of PdNPs and AuNPs.

Catalyst	A_{Pd}, cm^2	A_{Au}, cm^2
Pd_1Au_0	**1.36**	**0.00**
$Pd_1Au_{0.2}$	**1.30**	**0.08**
$Pd_1Au_{0.4}$	**0.92**	**0.34**
$Pd_1Au_{0.6}$	**0.36**	**0.58**
$Pd_1Au_{0.8}$	**0.15**	**0.68**
Pd_1Au_1	**0.08**	**0.74**

3.3. MOR: Catalytic activity and stability

The electrocatalytic activities toward MOR were examined by measuring the linear sweep voltammograms (LSVs) in 0.1 M NaOH solution containing 0.3 M methanol at a potential scan rate of 50 mV s^{-1} for the (a) Pd_1Au_0, (b) $Pd_1Au_{0.2}$, (c) $Pd_1Au_{0.4}$, (d) $Pd_1Au_{0.6}$, (e) $Pd_1Au_{0.8}$, and (f) Pd_1Au_1 catalysts (see Fig. 4). The I_p (assessing the catalytic enhancement) and E_{onset} (evaluating the unuseful polarizations) of the proposed catalysts are given in Table 2. Although all the prepared catalysts (Fig. 4b-f) showed improved activities toward MOR in comparison to the unmodified Pd/GC (Pd_1Au_0, Fig. 4a) catalyst, the Pd_1Au_1 catalyst (Fig. 4f) exhibited the highest catalytic activity in terms of I_p (1.53 mA cm^{-2}, i.e., ~ 12-fold) and the lowest E_{onset} (− 0.57 V). Table 3 presents a comparison between the electrochemical performance, in terms of I_p, of the catalysts included in this investigation and others reported in literature.

Bifunctional effects of PdNPs and AuNPs could be attributed to the considerable enhancement in the activity of the catalyst. The mechanism of MOR is given below [33]. The outstanding catalytic enhancement of AuNPs toward CO oxidation could significantly minimize the retention of adsorbed CO molecules at the Pd surface and that facilitated the MOR kinetics. The same mechanism indicated the regeneration of clean Pd and Au surfaces after the oxidative desorption of poisoning CO.

$$Pd + CH_3OH \rightarrow Pd\text{-}(CH_3OH)_{ads} \quad (1)$$

$$Pd\text{-}(CH_3OH)_{ads} \rightarrow Pd\text{-}(CO)_{ads} + 4H^+ + 4\,e^- \quad (2)$$

$$Au + H_2O \rightarrow Au\text{-}OH_{ads} + H^+ + e^- \quad (3)$$

$$Pd\text{-}(CO)_{ads} + Au\text{-}OH_{ads} \rightarrow Pd + Au + CO_2 + H^+ + e^- \quad (4)$$

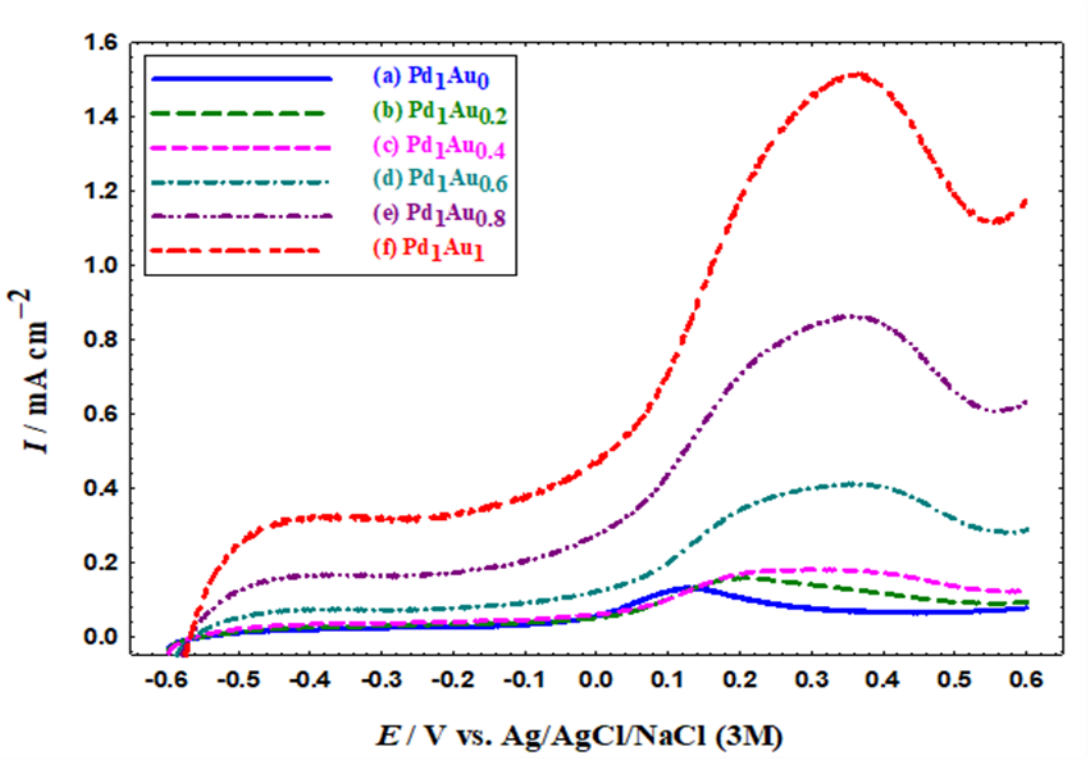

Figure 4. LSVs obtained at (a) Pd_1Au_0, (b) $Pd_1Au_{0.2}$, (c) $Pd_1Au_{0.4}$, (d) $Pd_1Au_{0.6}$, (e) $Pd_1Au_{0.8}$, and (f) Pd_1Au_1 catalysts in 0.1 M NaOH solution containing 0.3 M methanol. Potential scan rate = 50 mV s^{-1}.

Table 2. Electrochemical indices of the proposed catalysts (data were extracted from Fig. 4)

Catalyst	I_p / mA cm^{-2}	Enhancement factor = $\frac{I_p(catalyst)}{I_p(Pd_1Au_0)}$	E_{onset} / V
Pd_1Au_0	**0.13**	**1.0**	**− 0.521**
$Pd_1Au_{0.2}$	**0.16**	**1.2**	**− 0.533**
$Pd_1Au_{0.4}$	**0.18**	**1.4**	**− 0.552**
$Pd_1Au_{0.6}$	**0.42**	**3.2**	**− 0.554**
$Pd_1Au_{0.8}$	**0.88**	**6.8**	**− 0.573**
Pd_1Au_1	**1.53**	**11.8**	**− 0.571**

After assessing the electrocatalytic activity of the proposed catalysts toward MOR, it's highly important to estimate their catalytic stability. Figure 5 displays the current transients (*i*–*t* curves) obtained at the (a) Pd_1Au_0, (b) $Pd_1Au_{0.2}$, (c) $Pd_1Au_{0.4}$, (d) $Pd_1Au_{0.6}$, (e) $Pd_1Au_{0.8}$, and (f) Pd_1Au_1 catalysts in 0.1 M NaOH solution containing 0.3 M methanol at 0 V for 2700 s.

Table 3. A comparison of the electrocatalytic activities of several catalysts toward MOR.

Catalyst	Testing conditions	Activity (I_p / mA cm^{-2})	Ref
Pt/Ni(OH)$_2$/N-CNTs	0.1 M NaOH / 1.0 M CH_3OH, 50 mV s^{-1}, 25 °C	1.300	[48]
Pt/CNTs@C@Fe-Mo_2C	0.5 M H_2SO_4 / 1 M CH_3OH, 50 mV s^{-1}, 25 °C	1.439	[49]
Pt/Ti_3C_2 MXene	0.5 M H_2SO_4 / 0.5 M CH_3OH, 50 mV s^{-1}, 25 °C	1.137	[50]
Pt/Co@CS	0.5 M H_2SO_4 / 1.0 M CH_3OH, 50 mV s^{-1}, 25 °C	1.010	[51]
Pt@CS		0.880	
PdNPs/PVP-graphene	1.0 M NaOH / 0.5 M CH_3OH in, 50 mV s^{-1}, 25 °C	1.080	[52]
PdNPs/Vulcan		0.563	
Pt/C	1.0 M NaOH / 0.5 M CH_3OH in, 50 mV s^{-1}, 25 °C	0.520	[53]
Pd/C		0.690	
Pd_1Au_1/GC	0.1 M NaOH / 0.5 M CH_3OH in, 50 mV s^{-1}, 25 °C	1.530	This work

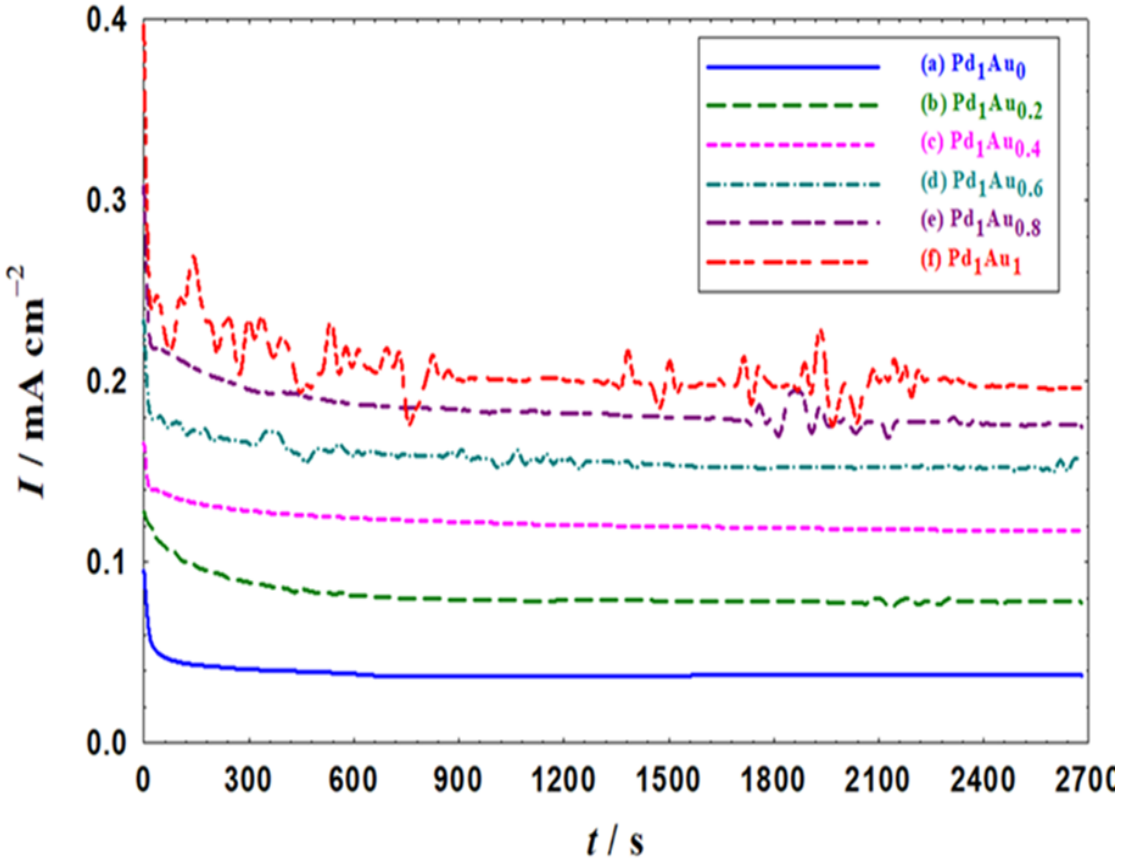

Figure 5. Current transients (*i-t*) measured at (a) Pd_1Au_0, (b) $Pd_1Au_{0.2}$, (c) $Pd_1Au_{0.4}$, (d) $Pd_1Au_{0.6}$, (e) $Pd_1Au_{0.8}$, and (f) Pd_1Au_1 catalysts in 0.1 M NaOH solution containing 0.3 M methanol. The stability curves recorded at a constant potential of 0.0 V.

The fastest decay and the lowest current, in agreement with previous investigations [33, 54, 55], was obviously noticed at the Pd_1Au_0 catalyst (Fig. 5a). This might arise from a possible poisoning for the Pd surface and/or a mechanical detachment or even a chemical dissolution of Pd during the long electrolysis [27]. Interestingly, a gradual increase in the current (obtained after the 2700 s electrolysis) was realized by increasing the amount of Au^{+3} ions in the deposition bath (from $Pd_1Au_{0.2}$ (Fig. 5b) to Pd_1Au_1 (Fig. 5f) catalyst). The best performance after 45 min of continuous electrolysis was obtained at the Pd_1Au_1 catalyst (0.2 mA cm^{-2}, i.e., 5 times that of the Pd_1Au_0 catalyst). This again confirmed the superiority of the proposed Pd_1Au_1 catalyst toward MOR.

4. CONCLUSION

Herein, PdAu alloyed catalysts were assembled via the simultaneous co-electrodeposition technique and were effectively recommended for MOR in alkaline media. The role of the Pd^{2+} and Au^{3+} molar ratio in the deposition bath on the catalytic performance (activity and stability) toward MOR was evaluated. Equimolar Pd^{2+} and Au^{3+} ions in the deposition bath was classified the optimum in this investigation. The Pd_1Au_1 catalyst acquired the highest catalytic activity (1.53 mA cm^{-2}, 11.8 enhancement factor and 50 mV negative shift in E_{onset} relative to the Pd_1Au_0 catalyst) and stability (5 times increase in I_p compared to that of the Pd_1Au_0 catalyst). The enhancement was thought to originate from facilitating the MOR kinetics via accelerating the oxidative CO removal by AuNPs.

References

1. S.D. Tilley, *Adv. Energy Mater*., 9 (2019) 1802877.
2. X. Wang, K. Wei, S. Yan, Y. Wu, J. Kang, P. Feng, S. Wang, F. Zhou, Y. Ling, *Appl. Catal. B: Environ*., 268 (2020) 118413.
3. C. Li, Q. Yuan, B. Ni, T. He, S. Zhang, Y. Long, L. Gu, X. Wang, *Nat. Commun*., 9 (2018) 3702.
4. I.M. Al-Akraa, T. Ohsaka, A.M. Mohammad, *Arab. J. Chem.*, 12 (2019) 897.
5. I.M. Al-Akraa, B.A. Al-Qodami, A.M. Mohammad, *Int. J. Electrochem. Sci*., 15 (2020) 4005.
6. I.M.Al-Akraa, B.A. Al-Qodami, M.S. Santosh, R. Viswanatha, A.K. Thottoli, A.M. Mohammad, *Int. J. Electrochem. Sci.*, 15 (2020) 5597.
7. I.M. Al-Akraa, Y.M. Asal, S.D. Khamis, *Int. J. Electrochem. Sci*., 13 (2018) 9712.
8. I.M. Al-Akraa, Y.M. Asal, A.M. Arafa, *Int. J. Electrochem. Sci*., 13 (2018) 8775.
9. I.M. Al-Akraa, A.E. Salama, Y.M. Asal, A.M. Mohammad, *Arab. J. Chem*., 14 (2021) 103383.
10. D. Wu, C. Wang, H. Wu, S. Wang, F. Wang, Z. Chen, T. Zhao, Z. Zhang, L.Y. Zhang, C.M. Li, *Carbon*, 163 (2020) 137.
11. I.M. Al-Akraa, Y.M. Asal, Aya A. Khalifa, *Int. J. Electrochem. Sci*., 14 (2019) 8276.
12. M. Abuzaied, Y.M. Asal , A.M. Mohammad, I.M. Al-Akraa, *Int. J. Electrochem. Sci*., 15 (2020) 2449.
13. I.M. Al-Akraa, A.M. Mohammad, *Arab. J. Chem*., 13 (2020) 4703.
14. A.S. Abdulhalim, Y.M. Asal, A.M. Mohammad, I.M. Al-Akraa, *Int. J. Electrochem. Sci*., 15 (2020) 3274.
15. I.M. Al-Akraa, Y.M. Asal, S.A. Darwish, *Int. J. Electrochem. Sci*., 14 (2019) 8267.
16. H. Xu, H. Shang, C. Wang, Y. Du, *Adv. Funct. Mater*., 30 (2020) 2000793.
17. M.K. Debe, *Nature*, 486 (2012) 43.
18. D.M. Fadzillah, S.K. Kamarudin, M.A. Zainoodin, M.S. Masdar, *Int. J. Hydrog. Energy*, 44 (2019)

3031.
19. R. Rath, P. Kumar, S. Mohanty, S.K. Nayak, *Int. J. Energy Res*., 43 (2019) 8931.
20. S. Ghosh, S. Bera, S. Bysakh, R.N. Basu, *Sustain. Energy Fuels*, 1 (2017) 1148.
21. T. Han, Z. Zhang, *Mater. Lett*., 154 (2015) 177.
22. M.S. El-Deab, G.H. El-Nowihy, A.M. Mohammad, *Electrochim. Acta*, 165 (2015) 402.
23. Y. Zhu, S.Y. Ha, R.I. Masel, *J. Power Sources*, 130 (2004) 8.
24. I.M. Sadiek, A.M. Mohammad, M.E. El-Shakre, M.S. El-Deab, B.E. El-Anadouli, *J. Solid State Chem.*, 17 (2013) 871.
25. I.M. Sadiek, A.M. Mohammad, M.E. El-Shakre, M.I. Awad, M.S. El-Deab, B.E. El-Anadouli, *Int. J. Electrochem. Sci*., 7 (2012) 3350.
26. Y.C. Liu, X.P. Qiu, Y.Q. Huang, W.T. Zhu, *Carbon*., 40 (2002) 2375.
27. I.M. Al-Akraa, A.M. Mohammad, M.S. El-Deab, B.E. El-Anadouli, *Int. J. Hydrog. Energy*, 40 (2015) 1789.
28. Y.M. Asal, I.M. Al-Akraa, A.M. Mohammad, M.S. El-Deab, *J. Taiwan Inst. Chem. Eng*., 96 (2019) 169.
29. Y.M. Asal, I.M. Al-Akraa, A.M. Mohammad, M.S. El-Deab, *Int. J. Hydrog. Energy*, 44 (2019) 3615.
30. R. Li, Z. Wei, T. Huang, A. Yu, *Electrochim. Acta*, 56 (2011) 6860.
31. M. Grdeń, M. Łukaszewski, G. Jerkiewicz, A. Czerwiński, *Electrochim. Acta*, 53 (2008) 7583.
32. C. Bianchini, P.K. Shen, *Chem. Rev*., 109 (2009) 4183.
33. R. Kottayintavida, N.K. Gopalan, *Electrochim. Acta*, 384 (2021) 138405.
34. C. Bock, C. Paquet, M. Couillard, G.A. Botton, B.R. MacDougall, *J Am Chem Soc*., 126 (2004) 8028.
35. S. Yang, Y. Chung, K.-S. Lee, Y. Kwon, *J Ind Eng Chem*., 90 (2020) 351.
36. T.-j. Hu, J. Zhao, W.-y. Jia, Y. Wang, J.-f. Jia, *J. Fuel Chem. Technol*., 49 (2021) 835.
37. X. Yu, D. Wang, Q. Peng, Y. Li, *Chem. Eur. J.*, 19 (2013) 233.
38. D. Martín-Yerga, G. Henriksson, A. Cornell, *Int. J. Hydrog. Energy*, 46 (2021) 1615.
39. Y. Bao, M. Zha, P. Sun, G. Hu, L. Feng, *J. Energy Chem*., 59 (2021) 748.
40. A. Caglar, M.S. Cogenli, A.B. Yurtcan, H. Kivrak, *Renew. Energy*, 150 (2020) 78.
41. M.G. Abd El-Moghny, H.H. Alalawy, A.M. Mohammad, A.A. Mazhar, M.S. El-Deab, B.E. El-Anadouli, *Int. J. Hydrog. Energy*, 42 (2017) 11166.
42. G.A. El-Nagar, M.S. El-Deab, A.M. Mohammad, B.E. El-Anadouli, *Electrochim. Acta*, 180 (2015) 268.
43. S. Trasatti, O.A. Petrii, *Pure Appl. Chem*., 63 (1991) 711.
44. M.S. El-Deab, L.A. Kibler, D.M. Kolb, *Electrochem. commun*., 11 (2009) 776.
45. I.M. Al-Akraa, A.M. Mohammad, M.S. El-Deab, B.E. El-Anadouli, *J. Nanotechnol*., 2018 (2018), 3803969.
46. I.M. Al-Akraa, Y.M. Asal, A.M. Mohammad, *J. Nanomater*., 2019 (2019), 784708.
47. I.M. Al-Akraa, A. Mohammad, M. El-Deab, B. El Anadouli, *Int. J. Electrochem. Sci*., 10 (2015) 3282.
48. Y. Wang, Y. Qin, X. Zhang, X. Dai, H. Zhuo, C. Luan, Y. Jiang, H. Zhao, H. Wang, X. Huang, *Dalton Trans*., 47 (2018) 7975.
49. S. Han, L. Ma, M. Gan, J. Shen, D. Wei, W. Zhan, J. Ding, C. Zhou, X. Zhong, *Appl. Surf. Sci*., 505 (2020) 144652.
50. Y. Wang, J. Wang, G. Han, C. Du, Q. Deng, Y. Gao, G. Yin, Y. Song, *Ceram. Int*., 45 (2019) 2411-2417.
51. S. Wei, F. Xie, M. Gan, L. Ma, T. Wu, Q. Fu, T. Li, Y. Yang, W. Zhan, *Synth. Met*., 280 (2021) 116878.
52. Y. Zhang, H. Shu, G. Chang, K. Ji, M. Oyama, X. Liu, Y. He, *Electrochim. Acta*, 109 (2013) 570.
53. X. Guo, Y. Tan, *Phys. Chem. Chem. Phys*., 17 (2015) 31956.

54. C. Wen, Y. Wei, D. Tang, B. Sa, T. Zhang, C. Chen, *Sci. Rep*., 7 (2017) 4907.
55. P. Hong, F. Luo, S. Liao, J. Zeng, *Int. J. Hydrog. Energy*, 36 (2011) 8518.